Materials Science and Engineering C 78 (2017) 619–626

Contents lists available at ScienceDirect

Materials Science and Engineering C

journal homepage: www.elsevier.com/locate/msec

Sustainable and smart keratin hydrogel with pH-sensitive swelling and enhanced mechanical properties

María Luz Peralta Ramos [a,b], Joaquín Antonio González [a,b], Lucas Fabian [b,c], Claudio Javier Pérez [d], María Emilia Villanueva [a,b], Guillermo Javier Copello [a,b,*]

[a] Universidad de Buenos Aires (UBA), Facultad de Farmacia y Bioquímica, Departamento de Química Analítica y Fisicoquímica, (UBA), Junín 956, C1113AAD Buenos Aires, Argentina
[b] Instituto de Química y Metabolismo del Fármaco, Fac. de Farmacia y Bioquímica, (IQUIMEFA-UBA-CONICET), Argentina
[c] Universidad de Buenos Aires (UBA), Facultad de Farmacia y Bioquímica, Cátedra de Química Medicinal, Argentina
[d] Instituto en Investigaciones en Ciencia y Tecnología de Materiales, Universidad de Mar del Plata, (CONICET), Juan B. Justo 4302, CP7600 Mar del Plata, Argentina

ARTICLE INFO

Article history:
Received 13 January 2017
Received in revised form 3 April 2017
Accepted 13 April 2017
Available online 21 April 2017

Keywords:
Keratin
Hydrogel
Biomaterial
Smart material
Stimuli-responsive

ABSTRACT

Protein based hydrogels are a very interesting type of biomaterials with many probed strengths related to their source and chemical structure. Biocompatibility and biodegradability are accompanied by affordability when it comes to low cost sources. The main keratin source is agroindustrial waste, such as feathers, horns, hooves, hair and wool. Thus, the main cost of keratin hydrogels derives from their processing. Here is presented a new strategy for the obtaining of a keratin hydrogel with enhanced mechanical properties using low cost reagents. This keratin hydrogel is stiff enough to allow handling without special cares and also presenting a reversible pH-responsive behavior. The minimum swelling is observed at low pH due to a collapsed and disordered protein network with water tightly adsorbed to the hydrophilic sites. The swelling rises significantly above pH 6 and the maximum swelling appears above pH 8 where an expanded network allows water to enter to the pores.

1. Introduction

Stimuli-responsive materials are those that react to a particular stimulus by changing a well-defined property of the original material. There have been reported varied stimuli that can trigger this change. Media pH, ionic strength, light intensity, temperature, electric and magnetic fields are the most commonly reported [1]. When these triggers are environmental changes these materials are prone to serve as sensors, whereas when the triggers can be precisely controlled these materials can be used as actuators. Literature presents a wide spectrum of technological application fields for stimuli-responsive materials. One of the main fields is medicine where smart biomaterials are thoroughly studied for drug delivery, wound dressing or tissue regeneration [1,2]. Nevertheless, there are numerous and varied applications for their use in sensor and actuator systems, such as swelling hydrogels for optical lenses or flow valves in microfluidic devices, piezoelectrics for sensing movement, or electro-actuating systems for controlled movement devices, among others [1,3,4].

Polymeric hydrogels consist in three dimensional networks which can contain up to 10 g water/g matrix without dissolving and many of them are responsive to environmental stimuli [5,6]. They may be formed by a single component, either unmodified or cross-linked, or by multiple components, such as interpenetrated polymer networks (IPN) or copolymers [7]. Biopolymer based hydrogels have recently gathered scientific and industrial attention and lead the efforts for the development of novel materials. This interest is driven by several properties typically present in these materials, such as biocompatibility, biodegradability and sometimes low cost, which lead to sustainability of the production process and high acceptability of the product by producers, consumers and regulation authorities [6,8–10].

Protein based hydrogels have also demonstrated the advantages of other biopolymers. The most widely studied protein based hydrogels have been obtained from collagen, fibrinogen, silk and elastin [11]. Particularly, keratin hydrogels are obtained by extraction of the soluble component of different low cost sources of this protein, such as feathers, hair, nails, wool, hoof, horn, etc. This extraction is mainly carried out by using an oxidant or a reductant giving origin to keratose or keratein respectively [12]. These extracts are filtered and dialyzed before the final gelling stage in which the keratin solution or material is obtained. Keratin materials thus prepared have been recently studied with biomedical purposes without reporting a stimuli-responsive property [13–16]. Up to date most reports make use of chemical grafting in order to endow keratin with stimuli-responsive behavior. Poly(*N*-(2-hydroxypropyl)methacrylamide) and poly(ethylene glycol) have been used to obtain smart materials in the micelle or nanoparticle form for

* Corresponding author at: Universidad de Buenos Aires (UBA), Facultad de Farmacia y Bioquímica, Departamento de Química Analítica y Fisicoquímica, (UBA), Junín 956, C1113AAD Buenos Aires, Argentina.
E-mail address: gcopello@ffyb.uba.ar (G.J. Copello).

http://dx.doi.org/10.1016/j.msec.2017.04.120
0928-4931/

their use in drug delivery [17–19]. Also, keratin materials have been obtained in the form of hydrogels and the grafting with methacrylic acid, *N*-isopropyl acrylamide and itaconic acid endowed the material with stimuli-responsive behavior [20–22].

Here we report the development of a smart keratin hydrogel with enhanced mechanical properties and stimuli-responsive behavior without the need of additional chemical graftings. This was achieved by using a new and sustainable route of synthesis. Reagents were kept to a minimum and aqueous salts and ethanol were used in order to aim for a green production process. Bovine horn was used as the source of keratin powder. The synthesis strategy was design to overcome two main issues of the traditional techniques: low protein recovery and long dialysis times. The swelling behavior of the hydrogel was analyzed by thoroughly studying the chemical and structural changes of the material. The reasons for this behavior were studied by different characterization techniques such as ATR-IR, Raman spectroscopy, NMR relaxometry, ss-NMR, DSC, SAXS, SEM and rheological behavior.

2. Experimental section

2.1. Materials

Sodium hydroxide, K_2HPO_4, KH_2PO_4 were purchased from Anedra (Argentina). Ethanol 96% was acquired from Soria (Avellaneda, Argentina). Ethyl Acetate was purchased from biopack (Argentina). Deuterated Chloroform was acquired from Sigma-Aldrich (St. Louis, USA). Phosphoric acid 85% from Mallinckrodt (USA). All other reagents were of analytical grade. A complete cow's horn (*Bos taurus*, Hereford) was used as keratin source.

2.2. Preparation of keratin materials

Horn was milled and sieved through a 250 μm sieve. Then, the horn powder was washed three times with distilled water, one time with ethanol and finally, three times with ethyl acetate to remove fat. After that, the powder were dried at 37 °C overnight. Keratin (1 g) powder was mixed with 7 ml dilution of NaOH 1 N in Ethanol (25 ml). The mixture was left at 45 °C for 4 h. After that, the mixture was homogenized through a syringe and left until complete dryness at 45 °C. This material was named: keratin block.

2.3. Swelled keratin hydrogel preparation

The keratin blocks obtained, were thoroughly washed with deonized water in order to remove all NaOH residue. After hydration, the hydrogel form of the material was obtained. For the achievement of different swelling ratios the hydrogels were equilibrated in a 10 mM phosphate solution ranging from pH 4 to pH 8. According of the equilibration pH the hydrogels were named as KerH-4, KerH-5, KerH-6, KerH-7 and KerH-8.

2.4. Swelling studies

In order to assess the swelling behavior of the material, 0.02 g of a keratin block were equilibrated in different 10 mM phosphate solutions ranging from pH 4 to pH 8. After equilibrium was reached, the hydrogels were removed from the solution and accurately weighted. The reversibility of the swelling behavior was determined by equilibrating and weighting the hydrogels in subsequent 10 mM phosphate solutions of pH 4 and then pH 8 and vice-versa.

2.5. Spectroscopic characterization

ATR-FTIR (diamond attenuated total reflectance) and FT-Raman spectra of washed horn powder, and keratin materials were recorded using a Nicolet iS50 Advanced Spectrometer (Thermo Scientific). ATR-FTIR spectra were recorded with 32 scans and a resolution of 4 cm^{-1}. FT-Raman spectra were acquired with an excitation laser beam of 1064 nm, 0.5 W laser power, resolution of 4 cm^{-1}, 50 scans. All samples were previously dried for 24 h at 60 °C to avoid water related bands interference.

The investigation of the ultrastructure of the hydrogels swelled at different pH was performed by Small Angle X-ray Scattering using the SAXS1 beamline of the National Synchrotron Light Laboratory (LNLS), Campinas, Brazil. The SAXS measurements were performed at room temperature in transmission geometry with $\lambda = 1.55$ Å (8 keV). The 2D SAXS spectra were monitored using a Pilatus 300 K detector. A sample to-detector distance of 0.9 and 3 m and an exposure time of 60 s were used. The samples were placed with their surfaces perpendicular to the direction of the incident X-ray beam and parallel to the X-ray detector. The scattering intensity (I) was measured as a function of the scattering vector (q) from 0.04 to 4.5 nm^{-1}. The background and parasitic scattering were determined by using an empty sample holder and were subtracted for each measurement.

Proton relaxation time experiments were performed in a Bruker UltraShield 600.13 MHz spectrometer with Avance III acquisition system, BOSS II shim system and Bruker SmartProbe BBO S3 with *Z*-gradient and automatic tune. Transverse relaxation curves for water spin-spin relaxation times (T_2) determination were obtained using a Carr-Purcell-Meiboom-Gill (CPMG) spin echo sequence [23]. The time spacing (τ) between pulses was varied between 0.1 and 100 ms.

The transverse magnetization decay curves were fitted using nonlinear least-squares analysis according to Eq. (1) [24]:

$$A(\tau)\sum_i A_{(i)} e^{\left(\frac{-\tau}{T_{2(i)}}\right)} + L_0 \quad (1)$$

where $A(\tau)$ is the signal intensity between even pairs of 180° pulses separated by a time τ, $A_{(i)}$ and $T_{2(i)}$ are the intensity and spin-spin relaxation time of component i, respectively, and L_0 is the decay curve baseline offset. Assuming only two components eq. 1 will turn in a second order exponential decay model.

Solid-state ^{13}C CP-MAS NMR (cross-polarization-magic angle spinning Nuclear Magnetic Resonance) spectra were performed on a Bruker Avance II-300 spectrometer equipped with a 4 mm MAS probe. All the NMR experiments were performed at room temperature. The operating frequency for carbons was 75.46 MHz and the spinning rate was 10 kHz. AQ: 41 ms, CT: 2 ms, repetition rate 5 s, NS: 2000.

2.6. Rheological behavior

The rheological behavior of the hydrogels swelled at different pH was studied. Amplitude sweeps were performed first in order to determine the linear viscoelastic range (LVR). The elastic or storage modulus, $G'(\omega)$, the viscous or loss modulus, $G''(\omega)$ and complex viscosity (η^*) of the studied materials were obtained in small-amplitude oscillatory shear flow experiments using a rotational rheometer from Anton Paar (MCR-301) provided with a CTD 600 thermo chamber. The tests were performed using parallel plates of 25 mm diameter and a frequency range of 0.1–500 s^{-1}. The measurements were carried out at room temperature (20 °C). All the tests were performed using small strains ($\gamma = 3.0\%$) to ensure the linearity of the dynamic responses [25]. All the runs were repeated using different samples. The gap width used was 700–800 μm.

2.7. Microscopic characterization

Electron microscopy images were obtained on a Zeiss Supra 40 scanning electron microscope (SEM). The hydrogels swelled at different pH were freeze-dried and coated with gold, before the observation.

2.8. Differential scanning calorimetry (thermal analysis)

Differential scanning calorimetry was performed using a Shimadzu DSC-50 device. The samples, previously freeze-dried, were tested from 20 °C to 260 °C at a heating rate of 10 °C/min, under nitrogen flow. Denaturation temperature (*Td*) and Tm were obtained from the curves.

2.9. Point of zero charge determination

The point of zero charge (pH_{pzc}) of the dry keratin material was determined by the drift method [26]. Briefly, a solution of 0.01 mol L^{-1} NaCl, was boiled to remove dissolved carbon dioxide and used to prepare several solutions with an initial pH ranging from 4 to 9. Then, 0.05 g of KerH was added to 10 ml of each solution and incubated at room temperature for 48 h. The final pH was measured and plotted against the initial pH. The pH point at which the curve of the final pH crosses the $pH_{initial} = pH_{final}$ line is the pH_{pzc}.

2.10. Statistics

All experiments and their corresponding measurements were conducted in triplicate under identical conditions and statistically analyzed by one-way ANOVA and by the Tukey Multiple comparison post-test if ANOVA $p < 0.05$. Data were expressed as means ± standard deviation (SD). A value of $p < 0.05$ was considered to be statistically significant. R language and environment was used for statistical computing and graphics [27].

3. Results

3.1. Spectroscopic characterization of the keratin blocks

Infrared and Raman spectroscopy were used with the aim of studying the changes suffered by the keratin powder in the obtaining process of the keratin blocks (dried hydrogels). By comparing the infrared spectra shown in Supplementary Data 1 (SD1) it could be seen that no appreciable changes in the keratin chemical structure arise in this stage. Nevertheless, the FT-Raman spectrum of the keratin block shows variations respecting the keratin powder spectrum (Fig. 1 and SD2). Firstly, the band corresponding to —S—S— bonds at 510 cm^{-1} present in the keratin powder spectrum is undetectable in the keratin block spectrum [28]. α-Keratins are structural, fibrous proteins that are held together by H-bonding and disulfide cross-linked bonds. The disulfide bridges enhance rigidity of the structure and contribute to the insolubility of keratin [29]. Thus, the breaking of —S—S— during the obtaining process would allow keratin chains to acquire higher mobility and let them rearrange in a different conformation respecting the powder. This endows the material with swelling capacity in the presence of water. Secondly, the before mentioned would be supported by the change in the symmetry of the amide I band at 1658 cm^{-1}. This band accounts for the overlapping of the bands corresponding to α-helix and β-sheets conformation of keratin, where peaks with maximums towards 1650 cm^{-1} correspond to the former and peaks towards 1670 cm^{-1} to the latter [28]. In this regard, the changes observed in this band would reinforce the assumption of a conformational change during the obtaining of the keratin blocks.

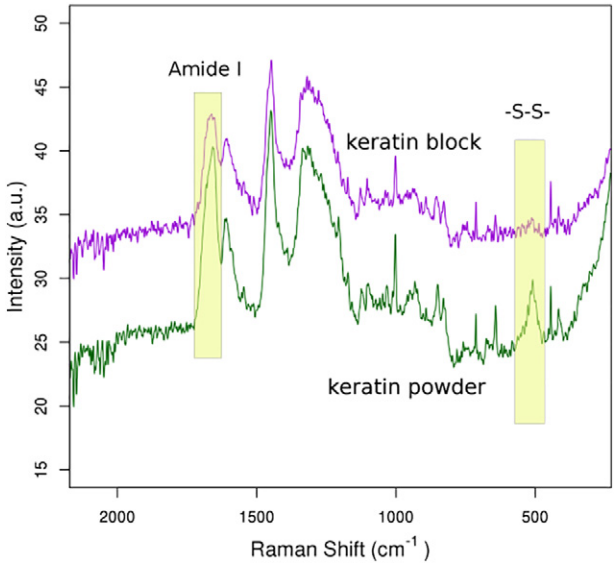

Fig. 1. FT-Raman spectra of keratin powder and keratin block.

3.2. Macroscopical characterization, swelling studies and point of zero charge determination

The dry keratin blocks present rigid structures that swell upon contact with water achieving a hydrogel form. The keratin hydrogels are stiff and compressible gels that can be easily handled, as can be seen in Fig. 2a. A reversible pH-responsive behavior was observed in the hydrogel form by equilibration between pH 4 and 8 as evidenced in Fig. 2a and c.

The hydrogel swelling properties were studied in order to assess its behavior at different media pH and its reversibility and the results are shown in Fig. 2b and c. As can be seen, at higher pHs (pH 6 to 8), the hydrogels present a higher swelling (up to 650%) than at low pH (around 100%). From low to high pHs, the swelling transition appears between pH 5 and 6 (KerH-5 and KerH-6) (significantly different $p < 0.01$, Tukey post-test). Although swelling at pH 8 and 7 (KerH-8 and KerH-7) is higher than at pH 6 (KerH-6), these swellings are significantly different with a $p < 0.05$ (significantly different $p < 0.01$, Tukey post-test). Since most basic aminoacids present their side chain groups *pKa* above pH 9, it could be considered that within the pH working range of this study, the protonation of these groups would remain unaltered. On the other hand, the acid aminoacids present their *pKa* around pH 4. Therefore, the main chemical changes would be related to these groups. Being the PZC of the keratin hydrogels 7.5 (SD3), it would be expected that below this point the material would present net positive charge. Remarkably, the swelling at low pHs was the lowest. Thus, electrostatic repulsion would be negligible as the driving mechanism for swelling.

With the aim to depict the hydrogels stimuli-responsive behavior and understand the mechanism involved, it was considered that keratin hydrogels present three types of structures associated with the swelling: 1) a low pH state (KerH-4 and KerH-5), 2) a high pH state (KerH-7 and KerH-8), and 3) a transition pH state at pH 6 (KerH-6). The following results will support this classification.

3.3. Microscopical characterization of the hydrogels

In order to study the microscopic topography of the hydrogels, they were freeze-dried and observed by SEM (Fig. 3). From the SEM images it can be observed that hydrogels equilibrated at low pH (KerH-4, KerH-5) and at the transition pH (KerH-6) present collapsed structures in comparison with the ones equilibrated at high pH (KerH-7 and KerH-8), which show an expanded topography with pores with diameter of few to several microns. At low pH the keratin structure is collapsed probably due to an interaction among keratin domains. At high pH, the chains expand to allow water to enter the pores. The latter could account for two main process. On one hand, interchain repulsion, but this would not be supported as it was mentioned before. On the other hand, the mechanism could imply a weakening of interchain interactions because of the loss of H-bonding and/or changes in the protein tertiary structure. Both would lead to the exposure of hydrophilic sites that allow the interaction with water and a subsequent pore filling.

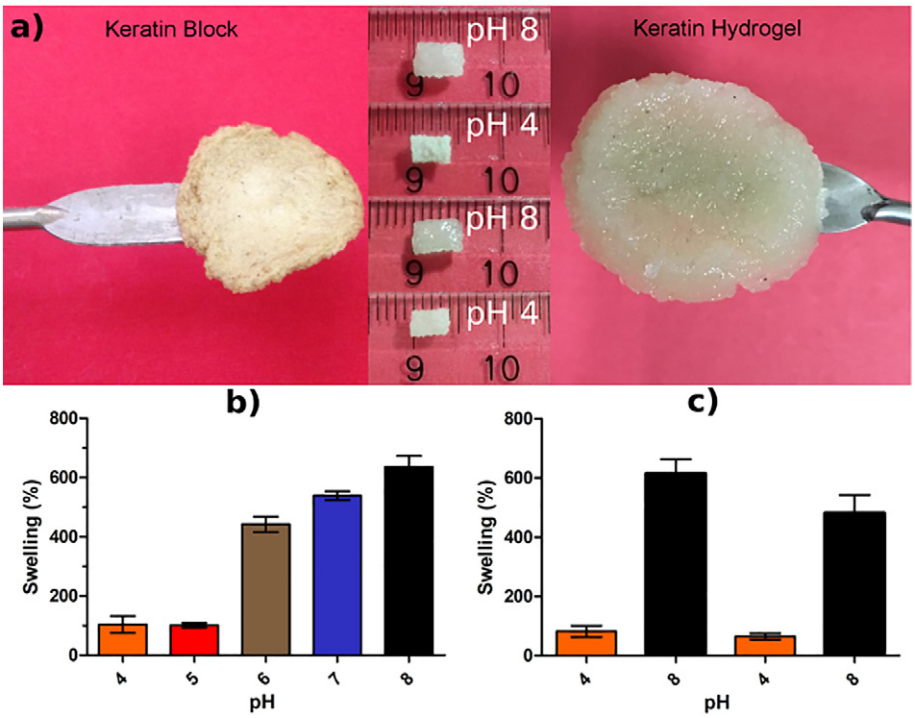

Fig. 2. a) Images of the keratin block, keratin hydrogel and pH responsiveness of the hydrogel (middle); b) Swelling behavior of the keratin hydrogels vs media pH; c) Reversibility of pH-responsiveness.

Interestingly, at the transition state (KerH-6) a more expanded network would be expected due to the swelling values. Nevertheless, a collapsed structure can be observed.

3.4. Thermal analysis (differential scanning calorimetry)

The thermal behavior of keratin powder and the hydrogels equilibrated at different pHs was studied by DSC. The thermograms are shown in Fig. 4a and the results are summarized in Table SD4. All samples showed an endothermic event around 110–130 °C. This peak accounts for bounded water evaporation, also known in literature as the denaturation temperature (*Td*) [30]. Since the main structure of the keratin do not suffer from extensive chemical modification, as observed from infrared spectra, it could be expected that water binding sites in the hydrogels remain similar to those in pristine keratin. Thus, the *Td* should be similar for all samples. On the other hand, the thermograms show differences among the keratin powder's and the hydrogels' temperature of melting (*Tm*), also seen as an endothermic event around 210–240 °C. As could be seen in Fig. 4a and Table SD4, keratin powder presents the higher *Tm*, whereas hydrogels equilibrated at low pH and at the transition pH show a *Tm* at 224–229 °C and those equilibrated at high pH present a *Tm* at 211–214 °C. This peak represents the denaturation of the protein and it has been used for the determination of the extent of structural modification [31,32]. Therefore, the changes

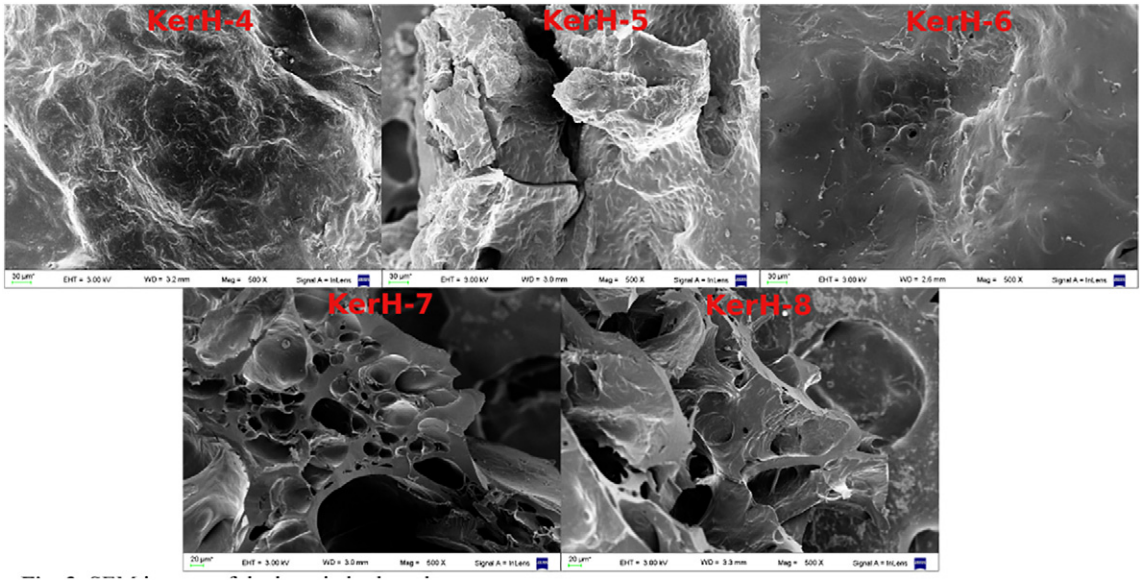

Fig. 3. SEM images of the keratin hydrogels.

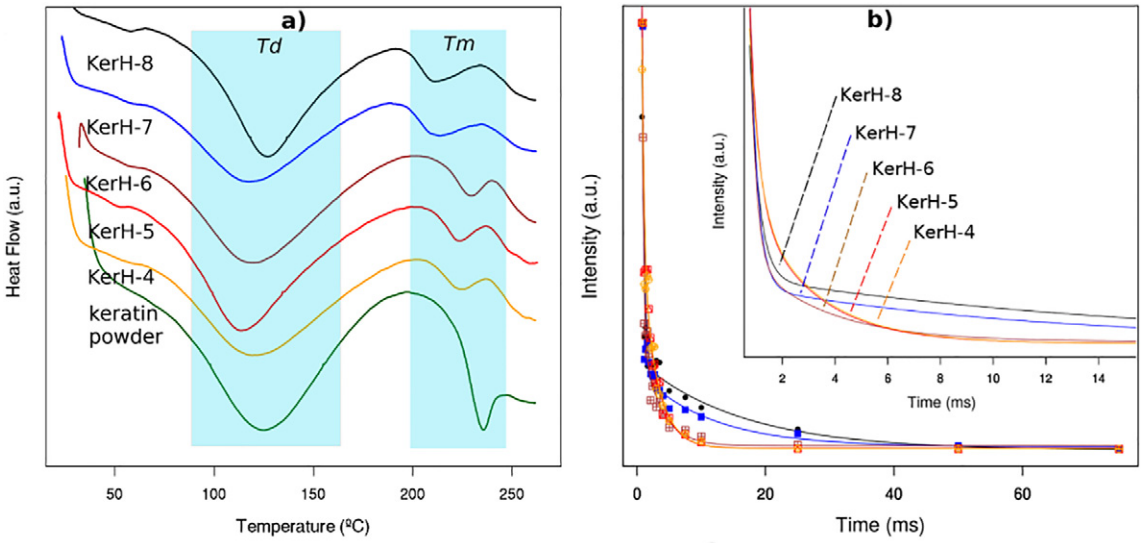

Fig. 4. DSC thermograms of the keratin powder and the hydrogels (a) and Transverse relaxation curves for water proton spin-spin relaxation (b).

seen in the *Tm* could also ascribe to the alteration of protein structures in the obtained hydrogels. Furthermore, the swelling process at different pHs would not only involve a water uptake variation by pore expansion/contraction but also conformational changes in the protein chains.

3.5. Water protons relaxation time determination

Transverse relaxation curves for water spin-spin relaxation time (T_2) of the hydrogels are presented in Fig. 4b. The shape of a spin relaxation curve is influenced by variations in the magnetic field that molecules are subjected to. Since molecular motion can affect the homogeneity of the magnetic field, it influences the relaxation curves shape. For free and randomly moving nuclei, such as water protons, relaxation time is typically in the order of seconds. On the other hand, when the same nuclei suffer a restricted motion their relaxation time becomes shorter, for instance when a molecule is located within a pore or interacting with a surface. In a system that both types of motion are present, both decay behaviors should be considered and each would be represented by an independent decay rate or spin-spin relaxation time (T_2) [33]. From the global decay of magnetization it could be seen that transverse relaxation of water protons is faster in KerH-4, KerH-5 and KerH-6 than for KerH-7 and KerH-8. Being the global decay of magnetization a contribution of all relaxations it could be proposed that the hydrogels would present two types of water regarding molecular motion. Since the values of T_2 calculated using Eq. (2) are considerably lower than 1 s, it was considered that the amount of free water is negligible in these hydrogels. This is probably due to the restriction of water to the pores and the high interaction with the protein hydrophilic groups. In this regard, Mc Conville et al., proposed that "bound" or motion restricted water can present two simple types of behavior regarding time scale, fast and slow, which other authors have assigned for poorly mobile or exchangeable water protons and bound water protons regarding their equilibrium between the adsorption surfaces and bulk solution [34,35]. The relaxation curves where fitted with a 2nd order exponential decay model considering the global contribution of a T_{2b} and a T_{2e}, accounting for bounded and exchangeable water protons respectively. As can be seen in Table SD5, all samples presented a T_{2b} in the same order of magnitude confirming that the behavior of the bound water to the hydrophilic sites of the protein is similar in all states. This could be expected since all hydrogels contain the same chemical structure and, therefore, the same water adsorption sites. On the other hand, the T_{2e} is similar for KerH-4, KerH-5 and KerH-6 but clearly higher for KerH-7 and KerH-8. This rise in T_{2e} for the high pH states can be explained by the higher swelling observed in this state which would imply higher water mobility. Nevertheless, this is contrasting with the KerH-6 T_{2e} value. KerH-6 presents a higher swelling that the low pH states but similar T_{2e}. This would be indicative that, although the material uptakes higher amounts of water at pH 6 than at low pHs, this exchangeable water do not present the same mobility that at higher pH states. Probably, at the transition state the water is taken by the material but adsorbed on the hydrophilic groups of keratin and, thus, its mobility is restricted. This model would imply that in the transition state conformational changes allow water to enter among the protein chains and be adsorbed allowing a transitional swelling.

3.6. Rheological behavior

Fig. 5 and SD6 show the rheological behavior of the hydrogels. G' was higher than G'' in all the samples, meaning that the elastic behavior of the material is predominant over the viscous component, a typical characteristic of a gel-like material [25]. Also, G' was higher in all samples (20 to 200 kPa) than other values reported in literature for pure keratin hydrogels obtained by the classical reduction method (1 to 10 kPa) [36,37].

Also, G' and the complex viscosity (η^*) decreased along with the pH of hydrogel equilibration (Fig. 5 and SD6). This performance is in concordance with the swelling assay results. At low pH, G' and η^* are high which is probably due to a strong interaction among keratin domains when its structure is collapsed. Upon swelling the keratin network expands and water enter to the pores, which diminishes G' and η^*. Also, the transition state (KerH-6) presents a distinctive behavior from the other samples showing a lower G' and η^* slopes with the increase of frequency, supporting the assumption that in this state the material conformation is different from the low and high pH states. A lower slope of G' would mean a higher cross-linking in this sample. Since no changes in the network cross-linking would be expected for this system, this could probably be due to the behavior of the transition pH state where keratin domains are reorganizing among states expressing a particular interaction.

3.7. Small angle X-ray scattering

The structural variations in the nanometric scale of the hydrogels at the different pH states, keratin blocks and keratin powder were studied by means of SAXS, as shown in Fig. 6. At low q ranges all samples follow a power-law behavior which is indicative of certain conformational

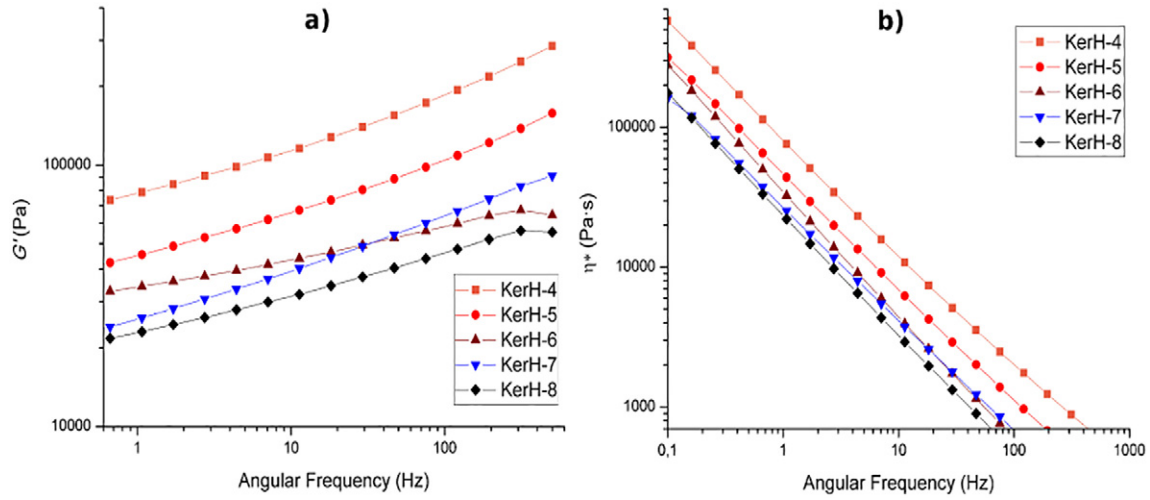

Fig. 5. Storage modulus (G′) (a) and complex viscosity (b) of the keratin hydrogels.

features for semicrystalline and disordered materials. Keratin powder and keratin blocks present this behavior in almost all the SAXS range, and fitted according to the relation $I(q)\sim q^{-\alpha}$, they show α values close to 4 which would account for surface fractals (Fig. 6a and Table SD7). In contrast, the hydrogels present lower α values. This was expected since lower values of this exponent would be related to lower network density [38–40]. The keratin blocks show a sharp correlation peak which according to Bragg's law ($d = 2\pi/q$) represents a distance of 4.6 nm. Being this peak absent in the keratin powder scattering profile, it indicates a conformational change during the partial hydrolysis process that, upon the final drying stage, would lead to a well ordered structure of keratin domains. Since this feature is absent in all the hydrogel samples, it can be inferred that swelling would endow the system with higher mobility and, thus, the loss of the semicrystalline conformation.

SAXS profiles for KerH-4 and KerH-5 samples show a power-law behavior up to 0.036 $Å^{-1}$, whereas in KerH-6, KerH-7 and KerH-8 this behavior is shorter and it is followed by a low α regime. This indicates that the keratin structure at the nanometric level is different at the low pH states than for the high pH states and the transitional pH state. Also, the α is lower for the former group of hydrogels than for the latter which is in accordance with the swelling assay where open network structures would be expected for higher swellings. In addition, the α value near to 1 of the middle regime would be related to a rod-like structure [41]. Since KerH-6, KerH-7 and KerH-8 clearly present multiple structural regimes, unlike the low pH states, in order to determine the local dimension of this conformation the scattering profiles of the transition and high pH states where modeled with the Beaucage unified equation for fractal materials with multiple structural levels [40,42]:

$$I(q) \approx G^{\left(\frac{-q^2R_g^2}{3}\right)} + B^{\left(\frac{-q^2R_{sub}^2}{3}\right)}\left(\frac{1}{q^*}\right)^P + G_s^{\left(\frac{-q^2R_s^2}{3}\right)} + B_s\left(\frac{1}{q_s^*}\right)^{P_s} \quad (2)$$

where G and G_s are the Guinier prefactors for the larger and smaller structures respectively, R_g is the radius of gyration, R_s is the smallest R_g observed at high q, whereas R_{sub} is at the high q limit, B and B_s are prefactors specific to the Power-law scattering, which are specified as the decay exponent P and P_s respectively, $q^* = q/[\mathrm{erf}\,(q\ k\ R_g/6^{1/2})]^3$ and $q_s^* = q/[\mathrm{erf}\,(q\ k_s\ R_s/6^{1/2})]^3$.

The modeled R_g values are presented as a inset table in Fig. 6b. As can be seen, all values are close which implies that the structural conformation of the transition pH state and the high pH state is similar or at least presents structures of the same spatial dimensions. In support of this assumption, the Kratky representation (Fig. 6b) shows similar profiles for KerH-6, KerH-7 and KerH-8. This representation is used for the determination of the folding state and flexibility of proteins and these profiles

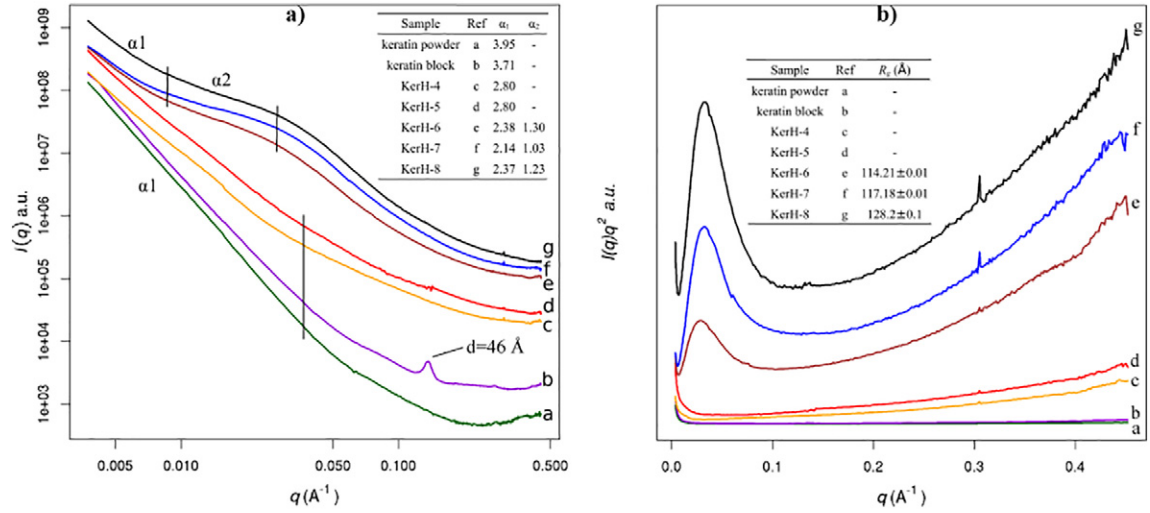

Fig. 6. SAXS profiles of the keratin powder, keratin block and keratin hydrogels. Log-log (a) and Kratky representation (b).

would indicate that the keratin at these pH values is folded or in a joint conformation of folded and disordered states [43]:

3.8. Solid-state ^{13}C NMR spectroscopy

Fig. 7 and SD8 present the CP-MAS ^{13}C NMR spectra for the keratin powder and the hydrogels. Supporting the FT-IR and FT-Raman analysis SD8 shows that the keratin chemical structure is maintained with no significant changes during the obtaining process. On the other hand, Fig. 7 shows that the peak corresponding to the amide carbonyl group at 175 ppm in the keratin powder spectrum shifts to 172–173 ppm in the hydrogels spectra. In proteins NMR spectra, the position of this peak accounts for the main-chain carbonyl carbon in the α-helix form when it is around 175–176 ppm, whereas account for the β-sheet form when it is around 172–173 ppm [44]. When a protein conformation involves both α-helix and β-sheet forms this peak results in the overlapping of both signals. The keratin powder spectra shows a clear maximum at 175 ppm together with a shoulder at 172 ppm which would account for both chain conformations in pristine keratin structure. On the contrary, this peak appears narrow and shifted to 172 ppm in the hydrogel spectra which would account mainly for a β-sheet conformation. Probably, during the obtaining process, after disulfide bridges are reduced, most of α-helix domains are lost without a significant alteration of the β-sheet domains. Also, upon pH rise, this peak slightly shifts towards 173 ppm. This would be due to the higher chain mobility of the more swelled states rather than a clear change in conformation.

4. Discussion

In order to depict the pH-responsive behavior of the keratin hydrogel, it can be proposed a dynamic model of water adsorption and protein reorganization, which is presented in Scheme 1. During the obtaining process, the breaking of the -S-S- bridges allows the α-helix in keratin to reorganize in flexible moieties that endow the final material with swelling capacity. In the hydrogel, at lower pH, the keratin structure is collapsed due to the presence of protonated –COOH which are able establish hydrogen bonds among the protein domains, mainly in a β-sheet conformation. At this condition the interdomain interaction is maximum. This leads to a material with low swelling, few pores, and a tight network which interacts with water only by adsorption to its hydrophilic sites.

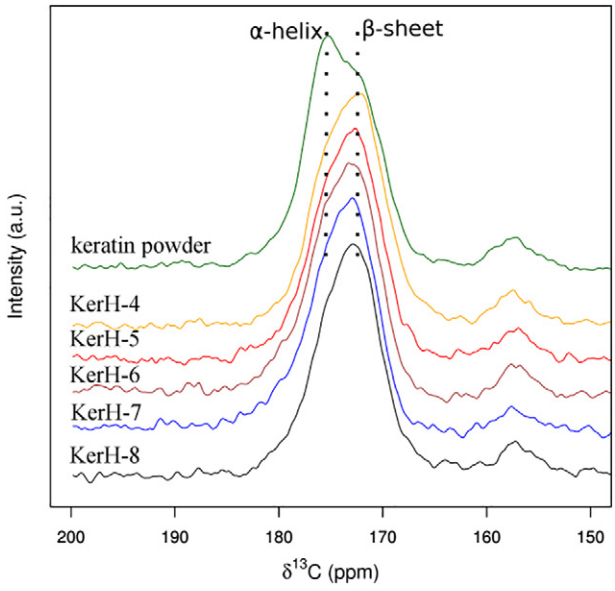

Fig. 7. Solid-state ^{13}C NMR spectra of keratin powder and the hydrogels.

At the transitional pH, the COO^- and the COOH groups are both present. Thus, hydrogen bonding density decays, more water adsorption sites become available and swelling increases. The adsorbed water in this state is still interacting with the surface of the protein. Nevertheless, this adsorption requires a distension of keratin chains leading to the expansion of the material implying a mayor reorganization. This reorganization would involve changes in flexible domains of the protein rather than a loss of the β-sheet conformation. Yet, in the transition state the structural change would not be sufficiently extended to be detected by SEM or DSC but the adsorbed water would be enough to be detected as a rise of swelling allowing the change in spatial organization confirmed by SAXS. In brief, this is a state that maintains some properties of the low pH states and express others from the high pH states.

On the other hand, at high pH states the —COO^- groups in the keratin structure would be hydrated rather than forming interchain hydrogen bonds. Hence, the main interaction would be due to a few interdomain interaction. Thus, higher structure associations would be disfavored allowing a higher swelling. As water enters to the network, the folded keratin associates would separate from other keratin associates giving place to larger pores. In this state water molecules can enter in the large pores and freely interact with the hydrophilic sites.

5. Conclusions

In this work a pH-responsive keratin hydrogel with enhanced mechanical properties has been obtained by a partial hydrolysis method. Two extreme states have been detected. One at low pH, for which swelling is minimum, and one at high pH, for which swelling is maximum. In both states the hydrogel is stiff enough to withstand handling with good mechanical properties, which is crucial for several applications. In addition, the material responsiveness is reversible. The obtaining process of the material would imply the reduction of the —S—S— bridges and the subsequent loss of most α-helix domains without appreciable loss of the β-sheet conformation. The mechanism of swelling in response to the media pH change would be a protein structural reorganization driven by carboxyl protonation/deprotonation rather than by electrostatic repulsion.

Acknowledgments

M.L.P.R. is grateful for an undergraduate fellowship granted by Universidad de Buenos Aires. M.E.V. is grateful for a postdoctoral fellowship granted by Consejo Nacional de Investigaciones Científicas y Técnicas (CONICET). J.A.G. is grateful for a doctoral fellowship granted by CONICET. This work was supported with grants from Universidad de Buenos Aires (UBACYT 20020130100780BA) and Agencia Nacional de Promoción Científica y Tecnológica (PICT 14-1919).

Appendix A. Supplementary data

Supplementary data to this article can be found online at http://dx.doi.org/10.1016/j.msec.2017.04.120.

References

[1] L. Ionov, Biomimetic hydrogel-based actuating systems, Adv. Funct. Mater. 23 (2013) 4555–4570, http://dx.doi.org/10.1002/adfm.201203692.
[2] B.M. Holzapfel, J.C. Reichert, J.-T. Schantz, U. Gbureck, L. Rackwitz, U. Nöth, F. Jakob, M. Rudert, J. Groll, D.W. Hutmacher, How smart do biomaterials need to be? A translational science and clinical point of view, Bionics - Biol. Inspired Smart Mater. 65 (2013) 581–603, http://dx.doi.org/10.1016/j.addr.2012.07.009.
[3] F.D. Jochum, P. Theato, Temperature- and light-responsive smart polymer materials, Chem. Soc. Rev. 42 (2013) 7468–7483, http://dx.doi.org/10.1039/C2CS35191A.
[4] H.C. Kim, S. Mun, H.-U. Ko, L. Zhai, A. Kafy, J. Kim, Renewable smart materials, Smart Mater. Struct. 25 (2016), 073001.
[5] V. Alzari, O. Monticelli, D. Nuvoli, J.M. Kenny, A. Mariani, Stimuli responsive hydrogels prepared by frontal polymerization, Biomacromolecules 10 (2009) 2672–2677, http://dx.doi.org/10.1021/bm900605y.

[6] M.E. Villanueva, A.M. del R. Diez, J.A. González, C.J. Pérez, M. Orrego, L. Piehl, S. Teves, G.J. Copello, Antimicrobial activity of starch hydrogel incorporated with copper nanoparticles, ACS Appl. Mater. Interfaces 8 (2016) 16280–16288, http://dx.doi.org/10.1021/acsami.6b02955.
[7] M.A. Haq, Y. Su, D. Wang, Mechanical properties of PNIPAM based hydrogels: a review, Mater. Sci. Eng. C 70 (Part 1) (2017) 842–855, http://dx.doi.org/10.1016/j.msec.2016.09.081.
[8] C. Rodríguez-González, A.L. Martínez-Hernández, V.M. Castaño, O.V. Kharissova, R.S. Ruoff, C. Velasco-Santos, Polysaccharide nanocomposites reinforced with graphene oxide and keratin-grafted graphene oxide, Ind. Eng. Chem. Res. 51 (2012) 3619–3629, http://dx.doi.org/10.1021/ie200742x.
[9] J.A. Gonzalez, M.F. Mazzobre, M.E. Villanueva, L.E. Diaz, G.J. Copello, Chitin hybrid materials reinforced with graphene oxide nanosheets: chemical and mechanical characterisation, RSC Adv. 4 (2014) 16480–16488, http://dx.doi.org/10.1039/C3RA47986B.
[10] M.L. Peralta Ramos, J.A. González, S.G. Albornoz, C.J. Pérez, M.E. Villanueva, S.A. Giorgieri, G.J. Copello, Chitin hydrogel reinforced with TiO2 nanoparticles as an arsenic sorbent, Chem. Eng. J. 285 (2016) 581–587, http://dx.doi.org/10.1016/j.cej.2015.10.035.
[11] A.L. Rutz, R.N. Shah, Protein-Based Hydrogels, in: S. Kalia (Ed.), Polym. Hydrogels Smart Biomater, Springer International Publishing, Cham 2016, pp. 73–104, http://dx.doi.org/10.1007/978-3-319-25322-0_4.
[12] P. Hill, H. Brantley, M. Van Dyke, Some properties of keratin biomaterials: kerateines, Biomaterials 31 (2010) 585–593, http://dx.doi.org/10.1016/j.biomaterials.2009.09.076.
[13] J.M. Saul, M.D. Ellenburg, R.C. de Guzman, M.V. Dyke, Keratin hydrogels support the sustained release of bioactive ciprofloxacin, J. Biomed. Mater. Res. A 98A (2011) 544–553, http://dx.doi.org/10.1002/jbm.a.33147.
[14] S. Xu, L. Sang, Y. Zhang, X. Wang, X. Li, Biological evaluation of human hair keratin scaffolds for skin wound repair and regeneration, Mater. Sci. Eng. C 33 (2013) 648–655, http://dx.doi.org/10.1016/j.msec.2012.10.011.
[15] M. Park, H.K. Shin, B.-S. Kim, M.J. Kim, I.-S. Kim, B.-Y. Park, H.-Y. Kim, Effect of discarded keratin-based biocomposite hydrogels on the wound healing process in vivo, Mater. Sci. Eng. C 55 (2015) 88–94, http://dx.doi.org/10.1016/j.msec.2015.03.033.
[16] F. Loan, S. Cassidy, C. Marsh, J. Simcock, Keratin-based products for effective wound care management in superficial and partial thickness burns injuries, Burns 42 (2016) 541–547, http://dx.doi.org/10.1016/j.burns.2015.10.024.
[17] Q. Li, L. Zhu, R. Liu, D. Huang, X. Jin, N. Che, Z. Li, X. Qu, H. Kang, Y. Huang, Biological stimuli responsive drug carriers based on keratin for triggerable drug delivery, J. Mater. Chem. 22 (2012) 19964, http://dx.doi.org/10.1039/c2jm34136k.
[18] Q. Li, S. Yang, L. Zhu, H. Kang, X. Qu, R. Liu, Y. Huang, Dual-stimuli sensitive keratin graft PHPMA as physiological trigger responsive drug carriers, Polym. Chem. 6 (2015) 2869–2878, http://dx.doi.org/10.1039/C4PY01750A.
[19] Y. Li, X. Zhi, J. Lin, X. You, J. Yuan, Preparation and characterization of DOX loaded keratin nanoparticles for pH/GSH dual responsive release, Mater. Sci. Eng. C 73 (2017) 189–197, http://dx.doi.org/10.1016/j.msec.2016.12.067.
[20] J. Guo, S. Pan, X. Yin, Y.-F. He, T. Li, R.-M. Wang, pH-sensitive keratin-based polymer hydrogel and its controllable drug-release behavior, J. Appl. Polym. Sci. 132 (2015) n/a-n/a 10.1002/app.41572.
[21] K. Sun, J. Guo, Y. He, P. Song, Y. Xiong, R.-M. Wang, Fabrication of dual-sensitive keratin-based polymer hydrogels and their controllable release behaviors, J. Biomater. Sci. Polym. Ed. 27 (2016) 1926–1940.
[22] T. Li, X. Yin, W. Zhai, Y.-F. He, R.-M. Wang, Enzymatic digestion of keratin for preparing a pH-sensitive biopolymer hydrogel, Aust. J. Chem. 69 (2016) 191–197.
[23] S. Meiboom, D. Gill, Modified spin-echo method for measuring nuclear relaxation times, Rev. Sci. Instrum. 29 (1958) 688–691.
[24] M. Ritota, R. Gianferri, R. Bucci, E. Brosio, Proton NMR relaxation study of swelling and gelatinisation process in rice starch–water samples, Food Chem. 110 (2008) 14–22, http://dx.doi.org/10.1016/j.foodchem.2008.01.048.
[25] J.D. Ferry, Viscoelastic Properties of Polymers, third ed. John Wiley & Sons, 1980.
[26] M.V. Lopez-Ramon, F. Stoeckli, C. Moreno-Castilla, F. Carrasco-Marin, On the characterization of acidic and basic surface sites on carbons by various techniques, Carbon 37 (1999) 1215–1221, http://dx.doi.org/10.1016/S0008-6223(98)00317-0.
[27] R Development Core Team, R: a language and environment for statistical computing, R Foundation for Statistical Computing, Vienna, Austria, http://www.R-project.org 2009.
[28] H.G. Edwards, D. Hunt, M. Sibley, FT-Raman spectroscopic study of keratotic materials: horn, hoof and tortoiseshell, Spectrochim. Acta A Mol. Biomol. Spectrosc. 54 (1998) 745–757, http://dx.doi.org/10.1016/S1386-1425(98)00013-4.
[29] L. Tombolato, E.E. Novitskaya, P.-Y. Chen, F.A. Sheppard, J. McKittrick, Microstructure, elastic properties and deformation mechanisms of horn keratin, Acta Biomater. 6 (2010) 319–330, http://dx.doi.org/10.1016/j.actbio.2009.06.033.
[30] P. Kakkar, B. Madhan, G. Shanmugam, Extraction and Characterization of Keratin From Bovine Hoof: A Potential Material for Biomedical Applications, 3, SpringerPlus, 2014 596, http://dx.doi.org/10.1186/2193-1801-3-596.
[31] C. Tonin, A. Aluigi, M. Bianchetto Songia, C. D'Arrigo, M. Mormino, C. Vineis, Thermoanalytical characterisation of modified keratin fibres, J. Therm. Anal. Calorim. 77 (2004) 987–996, http://dx.doi.org/10.1023/B:JTAN.0000041674.04961.b4.
[32] Q. Zhang, G. Shan, P. Cao, J. He, Z. Lin, Y. Huang, N. Ao, Mechanical and biological properties of oxidized horn keratin, Mater. Sci. Eng. C 47 (2015) 123–134, http://dx.doi.org/10.1016/j.msec.2014.11.051.
[33] B. Sierra-Martín, M.S. Romero-Cano, T. Cosgrove, B. Vincent, A. Fernández-Barbero, Solvent relaxation of swelling PNIPAM microgels by NMR, Liq. MesoSci. 270–271 (2005) 296–300, http://dx.doi.org/10.1016/j.colsurfa.2005.06.044.
[34] P. McConville, M.K. Whittaker, J.M. Pope, Water and polymer mobility in hydrogel biomaterials quantified by 1H NMR: a simple model describing both T1 and T2 relaxation, Macromolecules 35 (2002) 6961–6969, http://dx.doi.org/10.1021/ma020539c.
[35] L. Mengatto, M.G. Ferreyra, A. Rubiolo, I. Rintoul, J. Luna, Hydrophilic and hydrophobic interactions in cross-linked chitosan membranes, Mater. Chem. Phys. 139 (2013) 181–186, http://dx.doi.org/10.1016/j.matchemphys.2013.01.019.
[36] S. Wang, Z. Wang, S.E.M. Foo, N.S. Tan, Y. Yuan, W. Lin, Z. Zhang, K.W. Ng, Culturing fibroblasts in 3D human hair keratin hydrogels, ACS Appl. Mater. Interfaces 7 (2015) 5187–5198, http://dx.doi.org/10.1021/acsami.5b00854.
[37] J. Wang, S. Hao, T. Luo, Z. Cheng, W. Li, F. Gao, T. Guo, Y. Gong, B. Wang, Feather keratin hydrogel for wound repair: preparation, healing effect and biocompatibility evaluation, Colloids Surf. B: Biointerfaces 149 (2017) 341–350, http://dx.doi.org/10.1016/j.colsurfb.2016.10.038.
[38] S. Choudhary, S.R. Bhatia, Rheology and nanostructure of hydrophobically modified alginate (HMA) gels and solutions, Carbohydr. Polym. 87 (2012) 524–530, http://dx.doi.org/10.1016/j.carbpol.2011.08.025.
[39] C.J. Brinker, K.D. Keefer, D.W. Schaefer, R.A. Assink, B.D. Kay, C.S. Ashley, Sol-gel transition in simple silicates II, Glas. Glass Ceram. Gels. 63 (1984) 45–59, http://dx.doi.org/10.1016/0022-3093(84)90385-5.
[40] G. Beaucage, Small-angle scattering from polymeric mass fractals of arbitrary mass-fractal dimension, J. Appl. Crystallogr. 29 (1996) 134–146, http://dx.doi.org/10.1107/S0021889895011605.
[41] C. Schmitt, C. Moitzi, C. Bovay, M. Rouvet, L. Bovetto, L. Donato, M.E. Leser, P. Schurtenberger, A. Stradner, Internal structure and colloidal behaviour of covalent whey protein microgels obtained by heat treatment, Soft Matter 6 (2010) 4876, http://dx.doi.org/10.1039/c0sm00220h.
[42] G. Beaucage, Approximations leading to a unified exponential/power-law approach to small-angle scattering, J. Appl. Crystallogr. 28 (1995) 717–728, http://dx.doi.org/10.1107/S0021889895005292.
[43] P. Bernado, D.I. Svergun, Structural analysis of intrinsically disordered proteins by small-angle X-ray scattering, Mol. BioSyst. 8 (2012) 151–167, http://dx.doi.org/10.1039/C1MB05275F.
[44] H. Yoshimizu, I. Ando, Conformational characterization of wool keratin and S-(carboxymethyl)kerateine in the solid state by carbon-13 CP/MAS NMR spectroscopy, Macromolecules 23 (1990) 2908–2912, http://dx.doi.org/10.1021/ma00213a016.